THE ASTROPHYSICAL JOURNAL, 410:342–356, 1993 June 10

POLARIZATION ECLIPSE MODEL OF THE WOLF-RAYET BINARY V444 CYGNI WITH CONSTRAINTS ON THE STELLAR RADII AND AN ESTIMATE OF THE WOLF-RAYET MASS-LOSS RATE

N. ST-LOUIS,[1] A. F. J. MOFFAT,[1] L. LAPOINTE,[1] YU. S. EFIMOV,[2] N. M. SHAKHOVSKOY,[2]
G. K. FOX,[3] AND V. PIIROLA[4]

Received 1992 August 17; accepted 1992 November 11

ABSTRACT

We present an improved analytical model as well as a new set of multiwavelength observations of the polarization eclipse of the Wolf-Rayet binary V444 Cygni (WN5+O6). Comparing the model with the observations yields an estimate of the O and Wolf-Rayet star radii as well as of the Wolf-Rayet mass-loss rate. For the O star we find $R_{O*} = 8.5 \pm 1\ R_\odot$ and for the Wolf-Rayet star $R_{WR*} < 4\ R_\odot$. These values are in agreement with those derived by Cherepashchuk et al. from the detailed analysis of multiwavelength light curves.

For the Wolf-Rayet mass-loss rate we obtain $\dot{M} = 0.75 \times 10^{-5}\ M_\odot\ \mathrm{yr}^{-1}$, which is compatible with the dynamical values obtained from the rate of orbital period increase and with the value of $\dot{M}$ determined from the orbital double-wave modulation in polarization, but is at least 3 times smaller than the values derived from the free-free radio fluxes and modeling of infrared spectral lines. However, no allowance has been made in calculating the mass-loss rates for inhomogeneities, for which evidence is increasing in hot star winds. If the wind of the WR star in V444 Cygni is found to be clumpy, the radio/IR mass-loss rates are likely to be overestimated because of their dependency on the square of the density. In such a case, these values would probably have to be significantly decreased, bringing them closer to the polarization estimates, for which clumpy winds are irrelevant, providing the electron scattering remains optically thin.

Subject headings: binaries: eclipsing — polarization — stars: individual (V444 Cyg) — stars: Wolf-Rayet

1. INTRODUCTION

Wolf-Rayet (WR) stars are well-known for their substantial stellar winds, which are recognized as the strongest sustained outflows among all stable hot stars. These strong winds completely obscure the underlying core, rendering the determination of basic parameters such as radius and effective temperature extremely difficult. In the last decade, major improvements have been achieved in theoretical modeling of WR atmospheres (e.g., Hillier 1991a and references therein). Good agreement is generally found between observed and predicted continuum energy distributions as well as for the strengths and shapes of helium lines (Schmutz 1991). Carbon line strengths are also reproduced to better than a factor of 2 (Hillier 1989; Hamann et al. 1992). In spite of these important achievements, the winds of WR stars are still not well understood. In particular, the fundamental cause of their extremely high efficiency still remains to be identified.

In recent years, observations of the degree of polarization of the light from WR stars have been increasingly recognized as a new and useful tool for probing the nature of their dense, hot winds. The multitude of free electrons found in these ionized outflows constitutes the main source of polarization, by means of Thomson scattering of the light from the star. For WR+O binaries, the variation of the amount of linear polarization as a function of orbital phase is generally well understood. If one assumes spherical symmetry for the WR wind, the net polarization produced by the WR-star light will be zero but the polarization due to the scattering of the O-star light by the electrons in the WR wind will describe a double-wave curve over each orbital cycle. For circular orbits, the basic theoretical description for this type of variation was given by Rudy & Kemp (1978) and in more general form by Brown, McLean, & Emslie (1978, hereafter BME). The combination of this theory with good quality observations allows the determination of many system parameters, including the orbital inclination (which is otherwise available only from light-curve analyses of eclipsing binaries) and information on the distribution of wind material with respect to the orbital plane. Examples of applications of the BME theory to linear polarimetric observations of WR+O systems with circular orbits have recently been presented by many authors including Rudy & Kemp (1978), Luna (1982, 1985), Drissen et al. (1986a, b), St-Louis et al. (1987, 1988), Piirola & Linnaluoto (1988), Schulte-Ladbeck & van der Hucht (1989), and Robert et al. (1989, 1990). The theory of BME was extended to eccentric orbits by Brown et al. (1982). They found that for such systems, the polarization no longer describes a simple double-wave curve per orbital cycle but that first and third harmonic terms now become important, making the curve slightly more complex than in the case of a circular orbit. The model of Brown et al. (1982) has been applied to only two binaries so far. Both are WR+O systems, with eccentric orbits: γ Vel = HD 68237 (St-Louis et al. 1987) and WR 133 = HD 190918 (Robert et al. 1989).

In spite of the generally good agreement between observations and theory, examples of deviations from the model of BME for WR+O binaries have been noted. Drissen et al. (1987) and Robert et al. (1989) find a correlation between the level of random linear polarization variability and spectral

[1] Département de Physique, Université de Montréal, C.P. 6128, Succ. A, Montréal (Qc), H3C 3J7, Canada, and Observatoire du Mont Mégantic.
[2] Crimean Astrophysical Observatory, P/O Nauchny, 334413 Crimea, Ukraine.
[3] Department of Physics and Astronomy, University of Glasgow, Glasgow G12 8QQ, Scotland, UK.
[4] Observatory and Astrophysics Laboratory, University of Helsinki, Tähtitornmäki, SF-00130 Helsinki 13, Finland.

type for single WR stars, with later type stars showing the largest variations. These changes are attributed to intrinsic variations in the density or ionization structure of the WR wind itself. Therefore, it is not surprising that random-type variations are also observed superposed on the well-understood binary-induced polarization curves of WR + O systems (Drissen et al. 1987). In extreme cases, random variations are found to completely dominate and render the observation of the binary modulation extremely difficult (St-Louis et al. 1988).

Eclipsing WR binaries offer another example of deviation from the theory of BME. In this case, the discrepancy is caused by the weakening of direct light from the stars and to the occultation of varying amounts of scatterers by the finite-size disk of both stars. This effect was first predicted by Chandrasekhar (1946) in a slightly different context. In that paper, the author predicts that the radiation emerging from an atmosphere in which Thomson scattering by free electrons dominates the transfer of radiation is polarized at a level that varies from zero at the projected center of the star to 11% at the limb. The most favorable conditions to observe this effect are in an eclipsing binary where one of the stars is of early type. From lower inclination binaries, which present only atmospheric eclipses, the effect is likely to be undetectable, in view of the rapid decrease in electron density as a function of distance from the star. Among galactic WR stars, only three are known to be true core-eclipsing binaries: V444 Cyg, CQ Cep, and CX Cep; another is a possible candidate (GP Cep). The only other known core-eclipsing binary, HD 5980, is located in the Small Magellanic Cloud.

Robert et al. (1990) have reported the first detection for WR binaries of the effect predicted by Chandrasekhar in polarimetric observations of the best-known WR eclipsing binary, V444 Cyg (HD 193576, WR 139; WN 5 + O6). These authors have also presented a simple theoretical model to describe the variations. In spite of the very limited number of observations at eclipse (only six data points), Robert et al. (1990) were able to conclude that their fit of the model to the data was consistent with the small value of the core radius of the WR component (2.9 $R_\odot$) estimated from multiwavelength light curves by Cherepashchuk, Eaton, & Khaliullin (1984).

In this paper, we present a more comprehensive study of the polarization eclipse of V444 Cyg. An extensive data set of multicolor linear polarization observations has been obtained with particular emphasis on the eclipse of the WR star by the O-star companion. We also introduce a model with an improved treatment of the various occultation effects, compared to the model of Robert et al. (1990). Section 2 gives a brief description of the different occulted regions in a typical WR + O binary system such as V444 Cyg, as well as an account of which effects are included in the present calculations. In § 3 we discuss the observations; in § 4 the double-wave orbital modulation; and in § 5 we elaborate on the basis of the theoretical model. Finally, § 6 presents the results of the model fit to the observations, and § 7 gives a brief summary of our results.

2. THE EFFECTS OF THE OCCULTATION OF FREE ELECTRONS ON THE DEGREE OF POLARIZATION OF WOLF-RAYET BINARIES

One of the major approximations in the model of BME is to regard the stars as point sources. As a consequence, occultation effects are not taken into account. Scatterer occultation effects in binary systems have been considered by Brown & Fox (1989) and Fox & Brown (1991) in the somewhat artificial case of the companion star being negligible both in size and as a light source. They showed that when the envelope can be approximated to a plume of material, the density structure can be obtained from the polarimetric data. In real binary systems, however, both stars in general will be of finite size and contribute to the scattered flux. Figure 1 presents a rough sketch of the various occultated regions in a typical binary system. Four main areas must be examined: Region A_{WR} is the part of the envelope which is concealed (umbra) or only partly accessible (penumbra) to the O-star light, due to the finite size of the WR-star core. Similarly, A_O is the region of

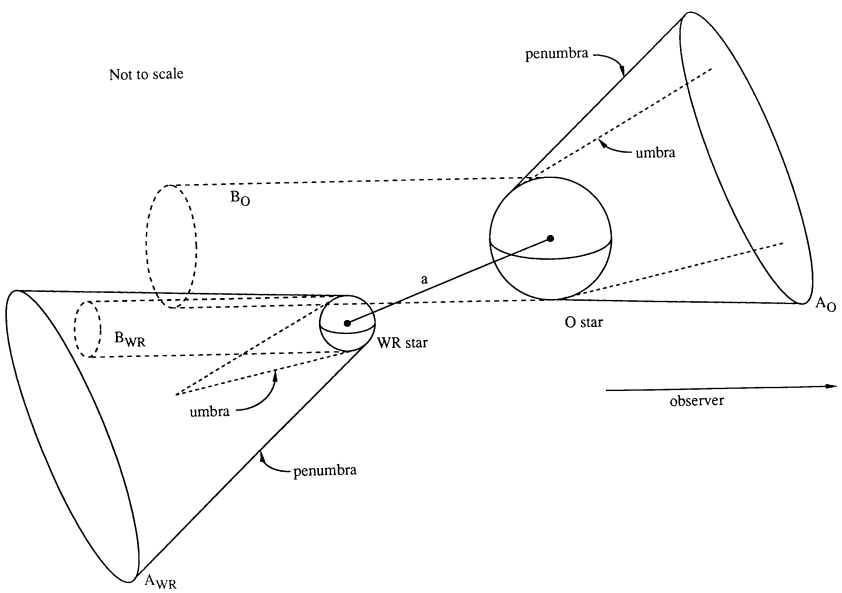

FIG. 1.—Cartoon of the various occulted regions in a typical binary system

the WR wind which is concealed to the WR-star light due to the O-star nucleus. To correctly account for regions A_O and A_{WR} would require one to allow for the nonsphericity of the light sources as seen by the electrons (cf. Fox 1992). However, providing the envelope is in corotation, these two regions will be stationary in the frame of the binary system. Therefore, viewed from a given star it is always *the same* number of scatterers which are occulted, whatever the orbital phase. The net effect is simply to reduce the total number of effective scatterers and thus the absolute value and amplitude of variation of the double-wave polarization curve. The shape of the curve as a function of orbital phase will be identical to that of a WR + O binary in which the WR component can be approximated by a point source with a spherically symmetric wind. In such a case, the variations of the observed polarization due to these two regions will be in accordance with the predictions of the BME model. Therefore, we have not included zones A_{WR} and A_O in the present calculations as we are solely interested in deviations from the BME model.

There are two remaining occulted regions. The first, B_{WR}, is the part of the envelope not visible to the observer because it is hidden by the core of the WR star and the second, B_O, is not visible because it is hidden by the O-star disk. These two regions are not stationary in the corotating frame. Instead, they scan through the WR-star wind, occulting varying amounts of scatterers and therefore producing polarization variations which deviate from the model of BME. These are the two main occultated regions which we must consider in the present model.

These two regions are responsible for four main effects: (i) The lack of visibility of the light from the WR star singly scattered off electrons in region B_{WR} and (ii) in region B_O, as well as (iii) light from the O star singly scattered off electrons in region B_{WR} and (iv) in region B_O. For simplicity, we shall consider that the wind of the WR star is spherically symmetric. Because of cylindrical symmetry with respect to the observer, effect (i) mentioned above always produces a net observed polarization of zero. Also, as the WR star has a much smaller radius ($R_{WR*} = 2.9\ R_\odot$: Cherepashchuk et al. 1984; $R_{O*} = 10\ R_\odot$: Cherepashchuk 1975), effect (iii) is negligible because of the relatively small number of scatterers involved, combined with dilution effects and occultation of some electrons by the WR core. Therefore, the only important region left to be considered is B_O, i.e., the main contributions to the level of polarization deviating from the BME model will come from the lack of observing the scattering of the WR and O-star light off electrons in the region eclipsed by the O star from the view of the observer. Hereafter, we will name this region the O-star shadow.

When adopting the point source approximation, not only does one incorrectly include in the calculations electrons which are occulted but one also inaccurately accounts for the incident direction of the radiation field. The effect of a finite disk on the resulting polarization has been formulated by Shulov (1967) and included for eclipse polarization computations by Piirola (1980). Recently, the effect of the finite size of the illuminating source was described theoretically by Cassinelli, Nordsieck, & Murison (1987). (See also a more general calculation by Brown, Carlaw, & Cassinelli 1989.) They find that for an electron at distance r, the polarization angle remains the same as for the point source approximation, but the degree of polarization is reduced by a factor $D = \cos\theta_*(r)$, where θ_* is the stellar angular radius of the disk seen at distance r. We shall include this effect in our calculations.

3. OBSERVATIONS

Some 70 individual observations in linear polarization were obtained during 1988/1989 in simultaneous *UBVRI* bands, using the five-channel polarimeter (Korhonen, Piirola, & Reiz 1984; Piirola 1988) at the 1.25 m telescope of the Crimean Astrophysical Observatory. During 1989 August, special emphasis was placed on observing around phases 0.5 ± 0.1, when the occultation effect on the polarization is most prominent. For each observation, Table 1 lists the Julian Date, the orbital phase calculated with the linear ephemeris of Khaliullin (1973) ($P = 4.212435$ days, $T_0 = 2441164.342$), and the Q and U Stokes parameters as well as their uncertainty, σ_p, for each filter. Generally, the total integration time (~ 15 minutes per data point) was chosen to yield a net precision of $\sigma_p \sim 0.03\%$ in B and R, the most efficient channels. Sometimes, however, this precision was not quite attained.

On one night (JD 2,447,767), during secondary eclipse, we also obtained a light curve simultaneously with the polarization. We used the same constant comparison star, c1, as in Moffat & Shara (1986).

4. THE DOUBLE-WAVE POLARIZATION ORBIT

The *UBVRI* polarization data are plotted versus orbital phase in Figure 2. As noted before by Robert et al. (1990), the rapid eclipse variations occur over phases 0.4–0.6. Thus, excluding the observations in this phase interval, we first fit the noneclipsing BME–type double-wave curve variations using the following equations:

$$Q = q_0 + q_1 \cos 4\pi\varphi + q_2 \sin 4\pi\varphi\ ,$$

$$U = u_0 + u_1 \cos 4\pi\varphi + u_2 \sin 4\pi\varphi\ ,$$

where φ is the orbital phase calculated using the linear ephemeris of Khaliullin (1973). A shift of -0.012 (cf. § 6) due mainly to a mass loss–generated period change (Khaliullin, Khaliullina, & Cherepashchuk 1984) was added to these phases. The fits are also shown in Figure 2. Table 2 gives the parameters (cf. BME) from these fits in each filter. Note that: (*a*) the orbital inclination, (*b*) the longitude of nodes, Ω, and (*c*) the semimajor axis of the ellipse, A_p, described in the Q–U plane by this binary system are independent of wavelength. (*d*) The scattering moment $\tau_0\gamma_3$ (cf. BME) also shows no correlation with wavelength and is compatible with that of Robert et al. (1990). (*e*) The complementary moment $\tau_0\gamma_4$ is generally insignificantly different from zero (as is $\lambda_2 = \frac{1}{2}\tan^{-1}\gamma_4/\gamma_3$). This implies that the double-wave scattering function arises in electrons centered on at least one of the stars, most likely mainly the strong-wind WR star. This result for $\tau_0\gamma_4$ and λ_2 differs from that of Robert et al. (1990), who did not allow for a period change. (*f*) The amplitude of double-wave polarization variability is not correlated with wavelength, as expected for electron scattering. However, detectable wavelength dependence may be masked by noise introduced by the fact that some filters (especially *B*) are more sensitive than others to depolarization in the emission lines (cf. Moffat & Piirola 1993 for other WR + O binaries).

As there is no noticeable dependence of the polarization variations with wavelength, we have combined the linear polarimetric observations from the various filters by using the individual uncertainties as weighting factors. We have subsequently fitted a double-wave BME–type curve to the averaged data. The orbital inclination fitted to the weighted mean data (last column in Table 2), $i = 80\overset{\circ}{.}8 \pm 1\overset{\circ}{.}6$, is insignificantly larger

TABLE 1

LINEAR POLARIZATION OBSERVATIONS OF V444 CYGNI

Julian Date 2447000+	Orbital Phase	U Filter Q	U Filter U	U Filter σ_P	B Filter Q	B Filter U	B Filter σ_P	V Filter Q	V Filter U	V Filter σ_P	R Filter Q	R Filter U	R Filter σ_P	I Filter Q	I Filter U	I Filter σ_P
320.384	0.397	+0.137	−0.398	0.032	+0.123	−0.398	0.033	+0.149	−0.449	0.029	+0.108	−0.300	0.018	+0.156	−0.268	0.029
321.436	0.647	+0.116	−0.528	0.032	+0.124	−0.651	0.043	+0.145	−0.598	0.031	+0.126	−0.504	0.026	+0.156	−0.461	0.021
323.367	0.105	+0.139	−0.369	0.049	+0.199	−0.418	0.037	+0.215	−0.436	0.070	+0.279	−0.273	0.023	+0.267	−0.216	0.045
324.370	0.343	+0.217	−0.383	0.042	+0.237	−0.504	0.049	+0.284	−0.409	0.019	+0.289	−0.352	0.021	+0.275	−0.324	0.024
325.367	0.580	+0.145	−0.467	0.078	+0.101	−0.283	0.080	+0.177	−0.315	0.063	+0.224	−0.273	0.066	+0.175	−0.245	0.044
326.383	0.821	+0.232	−0.195	0.121	+0.313	−0.437	0.044	+0.232	−0.426	0.074	+0.331	−0.305	0.054	+0.328	−0.264	0.036
329.383	0.533	+0.069	−0.318	0.078	+0.204	−0.315	0.037	+0.160	−0.231	0.029	+0.152	−0.189	0.030	+0.131	−0.157	0.037
333.383	0.483	−0.181	−0.371	0.086	−0.104	−0.400	0.055	−0.105	−0.382	0.071	−0.061	−0.305	0.035	−0.013	−0.303	0.029
335.419	0.966	+0.165	−0.250	0.108	−0.013	−0.276	0.031	+0.053	−0.277	0.077	+0.141	−0.188	0.035	+0.071	−0.248	0.016
338.338	0.659	+0.050	−0.570	0.067	+0.117	−0.550	0.027	+0.195	−0.525	0.050	+0.195	−0.426	0.019	+0.223	−0.339	0.041
339.334	0.896	+0.211	−0.372	0.046	+0.160	−0.382	0.037	+0.092	−0.324	0.043	+0.197	−0.242	0.017	+0.145	−0.232	0.027
341.514	0.413	−0.460	+0.081	0.132	−0.015	−0.101	0.046	+0.182	−0.138	0.054	+0.222	−0.083	0.044	+0.180	−0.070	0.039
347.339	0.796	+0.168	−0.655	0.050	+0.269	−0.507	0.038	+0.274	−0.494	0.040	+0.275	−0.370	0.023	+0.233	−0.331	0.028
348.335	0.032	−0.023	−0.389	0.065	+0.065	−0.352	0.031	−0.048	−0.303	0.056	+0.054	−0.225	0.024	+0.091	−0.248	0.024
349.330	0.269	+0.348	−0.579	0.052	+0.241	−0.557	0.036	+0.337	−0.574	0.054	+0.300	−0.496	0.026	+0.299	−0.454	0.032
434.307	0.441	+0.061	−0.188	0.050	+0.058	−0.266	0.029	+0.068	−0.249	0.033	+0.122	−0.209	0.027	+0.165	−0.116	0.049
435.298	0.677	+0.141	−0.504	0.033	+0.220	−0.504	0.028	+0.218	−0.533	0.033	+0.231	−0.439	0.018	+0.230	−0.411	0.034
437.287	0.149	+0.137	−0.399	0.030	+0.121	−0.369	0.026	+0.137	−0.436	0.038	+0.211	−0.381	0.025	+0.200	−0.331	0.022
439.328	0.633	+0.060	−0.449	0.024	+0.127	−0.441	0.033	+0.118	−0.479	0.035	+0.177	−0.446	0.025	+0.164	−0.354	0.034
442.242	0.325	+0.228	−0.367	0.032	+0.271	−0.424	0.018	+0.349	−0.393	0.026	+0.327	−0.374	0.018	+0.307	−0.344	0.016
447.285	0.522	+0.139	−0.164	0.040	+0.166	−0.281	0.045	+0.158	−0.173	0.076	+0.212	−0.319	0.072	+0.264	−0.231	0.062
451.239	0.461	−0.129	−0.235	0.029	−0.058	−0.285	0.032	−0.024	−0.281	0.032	+0.014	−0.259	0.026	+0.013	−0.238	0.029
458.258	0.127	+0.029	−0.272	0.092	+0.116	−0.411	0.056	−0.070	−0.398	0.096	+0.052	−0.378	0.048	+0.045	−0.278	0.096
689.393	0.997	+0.056	−0.314	0.054	−0.007	−0.226	0.036	+0.110	−0.236	0.029	+0.057	−0.190	0.018	+0.078	−0.225	0.038
690.412	0.239	+0.339	−0.560	0.045	+0.296	−0.478	0.027	+0.423	−0.500	0.036	+0.354	−0.413	0.020	+0.366	−0.449	0.034
695.399	0.423	+0.096	−0.230	0.061	+0.167	−0.166	0.023	+0.195	−0.266	0.046	+0.199	−0.195	0.030	+0.108	−0.184	0.028
729.358	0.484	−0.217	−0.370	0.032	−0.073	−0.373	0.029	−0.074	−0.360	0.038	−0.035	−0.365	0.028	−0.019	−0.239	0.024
730.338	0.717	+0.201	−0.596	0.041	+0.213	−0.537	0.022	+0.260	−0.552	0.033	+0.250	−0.440	0.030	+0.206	−0.412	0.029
759.327	0.599	+0.097	−0.314	0.092	+0.134	−0.294	0.033	+0.099	−0.441	0.040	+0.031	−0.367	0.024	+0.003	−0.251	0.045
760.363	0.844	+0.268	−0.460	0.056	+0.247	−0.316	0.022	+0.324	−0.456	0.033	+0.325	−0.421	0.038	+0.298	−0.310	0.026
761.499	0.114	+0.049	−0.588	0.131	+0.166	−0.314	0.045	+0.130	−0.369	0.035	+0.255	−0.306	0.052	+0.260	−0.270	0.055
762.435	0.336	+0.353	−0.519	0.055	+0.312	−0.430	0.033	+0.301	−0.530	0.041	+0.369	−0.428	0.027	+0.323	−0.341	0.023
763.261	0.532	+0.026	−0.164	0.079	+0.216	−0.219	0.052	+0.292	−0.159	0.059	+0.203	−0.173	0.033	+0.169	−0.142	0.041
763.318	0.546	+0.149	−0.113	0.075	+0.185	−0.204	0.056	+0.215	−0.141	0.050	+0.161	−0.162	0.021	+0.121	−0.065	0.033
763.377	0.560	+0.061	−0.152	0.071	+0.075	−0.181	0.037	+0.098	−0.180	0.055	+0.077	−0.160	0.037	+0.085	−0.110	0.038

TABLE 1—*Continued*

Julian Date 2447000+	Orbital Phase	U Filter Q	U	σ_P	B Filter Q	U	σ_P	V Filter Q	U	σ_P	R Filter Q	U	σ_P	I Filter Q	U	σ_P
763.460	0.580	−0.088	−0.221	0.071	+0.019	−0.278	0.053	−0.004	−0.293	0.044	+0.060	−0.225	0.047	+0.013	−0.184	0.039
764.419	0.807	+0.178	−0.494	0.077	+0.324	−0.412	0.045	+0.335	−0.475	0.049	+0.231	−0.348	0.042	+0.266	−0.358	0.040
765.513	0.067	−0.118	−0.331	0.094	+0.120	−0.349	0.050	+0.043	−0.333	0.056	+0.027	−0.355	0.068	+0.178	−0.291	0.068
766.403	0.278	+0.292	−0.593	0.092	+0.341	−0.501	0.084	+0.190	−0.551	0.080	+0.189	−0.417	0.093	+0.253	−0.317	0.090
767.271	0.484	−0.142	−0.301	0.084	−0.094	−0.372	0.023	−0.088	−0.407	0.045	−0.029	−0.336	0.040	−0.084	−0.260	0.033
767.288	0.488	−0.130	−0.499	0.062	+0.021	−0.348	0.036	−0.004	−0.400	0.057	−0.009	−0.309	0.021	+0.022	−0.269	0.027
767.305	0.492	−0.049	−0.486	0.046	+0.019	−0.361	0.038	+0.059	−0.393	0.034	+0.032	−0.350	0.043	+0.038	−0.326	0.039
767.323	0.497	+0.120	−0.336	0.069	+0.051	−0.370	0.044	+0.171	−0.238	0.041	+0.106	−0.344	0.030	+0.124	−0.266	0.037
767.339	0.501	−0.026	−0.315	0.054	+0.157	−0.333	0.030	+0.145	−0.394	0.058	+0.151	−0.326	0.026	+0.142	−0.304	0.034
767.356	0.505	+0.064	−0.240	0.064	+0.102	−0.342	0.036	+0.042	−0.427	0.057	+0.132	−0.337	0.053	+0.110	−0.321	0.031
767.377	0.510	+0.048	−0.244	0.104	+0.141	−0.340	0.052	+0.091	−0.302	0.054	+0.145	−0.244	0.046	+0.202	−0.195	0.044
767.395	0.514	+0.027	−0.248	0.087	+0.205	−0.334	0.045	+0.183	−0.328	0.059	+0.174	−0.264	0.047	+0.226	−0.126	0.044
767.412	0.518	+0.195	−0.468	0.109	+0.125	−0.366	0.052	+0.189	−0.272	0.051	+0.193	−0.288	0.038	+0.130	−0.163	0.037
767.429	0.522	+0.083	−0.287	0.076	+0.176	−0.263	0.039	+0.243	−0.394	0.053	+0.247	−0.234	0.042	+0.248	−0.230	0.038
767.448	0.526	+0.059	−0.115	0.095	+0.251	−0.271	0.050	+0.291	−0.224	0.061	+0.326	−0.119	0.040	+0.202	−0.199	0.041
767.468	0.531	+0.192	−0.412	0.045	+0.250	−0.193	0.048	+0.369	−0.268	0.043	+0.314	−0.193	0.048	+0.349	−0.178	0.034
767.486	0.535	+0.291	−0.362	0.085	+0.359	−0.224	0.052	+0.242	−0.124	0.056	+0.248	−0.196	0.036	+0.271	−0.049	0.038
767.509	0.541	+0.387	−0.245	0.120	+0.225	−0.069	0.060	+0.308	−0.154	0.051	+0.204	−0.045	0.056	+0.255	−0.005	0.053
767.535	0.547	−0.039	+0.152	0.243	+0.203	−0.148	0.060	+0.208	−0.139	0.057	+0.269	−0.138	0.058	+0.160	−0.115	0.064
768.392	0.751	+0.275	−0.558	0.028	+0.313	−0.528	0.023	+0.292	−0.578	0.030	+0.340	−0.464	0.025	+0.329	−0.470	0.022
784.315	0.531	+0.153	−0.091	0.064	+0.233	−0.148	0.060	+0.233	−0.171	0.040	+0.215	−0.176	0.029	+0.240	−0.161	0.029
784.345	0.538	+0.268	+0.018	0.091	+0.215	−0.135	0.045	+0.209	−0.176	0.059	+0.173	−0.130	0.045	+0.220	−0.063	0.039
784.365	0.542	+0.108	−0.194	0.081	+0.225	−0.056	0.032	+0.183	−0.055	0.039	+0.191	−0.063	0.033	+0.157	−0.035	0.040
784.392	0.549	+0.191	−0.166	0.072	+0.196	−0.113	0.037	+0.225	−0.044	0.039	+0.179	−0.150	0.048	+0.184	−0.064	0.043
788.299	0.476	−0.208	−0.388	0.154	−0.013	−0.318	0.056	−0.140	−0.348	0.093	−0.013	−0.310	0.042	−0.038	−0.235	0.030
788.448	0.512	+0.058	−0.275	0.057	+0.117	−0.287	0.024	+0.117	−0.295	0.041	+0.111	−0.304	0.033	+0.109	−0.228	0.027
788.484	0.520	+0.229	−0.179	0.089	+0.209	−0.226	0.030	+0.232	−0.171	0.031	+0.138	−0.238	0.030	+0.153	−0.203	0.036
792.259	0.416	+0.163	−0.273	0.040	+0.188	−0.254	0.029	+0.174	−0.236	0.033	+0.125	−0.210	0.021	+0.138	−0.186	0.024
792.286	0.423	+0.209	−0.240	0.037	+0.145	−0.253	0.023	+0.214	−0.220	0.033	+0.154	−0.236	0.027	+0.108	−0.148	0.025
792.311	0.429	+0.113	−0.288	0.023	+0.122	−0.264	0.024	+0.200	−0.279	0.036	+0.108	−0.262	0.020	+0.120	−0.205	0.033
792.329	0.433	+0.080	−0.237	0.062	+0.229	−0.323	0.052	+0.217	−0.253	0.032	+0.116	−0.257	0.023	+0.146	−0.236	0.021
792.350	0.438	+0.088	−0.164	0.041	+0.128	−0.238	0.029	+0.191	−0.294	0.032	+0.102	−0.246	0.025	+0.087	−0.204	0.032
792.378	0.445	+0.065	−0.255	0.042	+0.113	−0.243	0.014	+0.088	−0.238	0.032	+0.086	−0.243	0.018	+0.046	−0.240	0.021
792.403	0.451	+0.054	−0.212	0.052	+0.016	−0.251	0.029	+0.089	−0.199	0.040	+0.025	−0.229	0.030	+0.029	−0.185	0.028
792.428	0.456	+0.028	−0.212	0.033	+0.008	−0.221	0.029	+0.004	−0.241	0.040	+0.033	−0.259	0.027	+0.041	−0.185	0.022
792.449	0.461	−0.006	−0.328	0.052	+0.002	−0.230	0.034	+0.083	−0.278	0.058	−0.019	−0.252	0.035	+0.001	−0.205	0.027

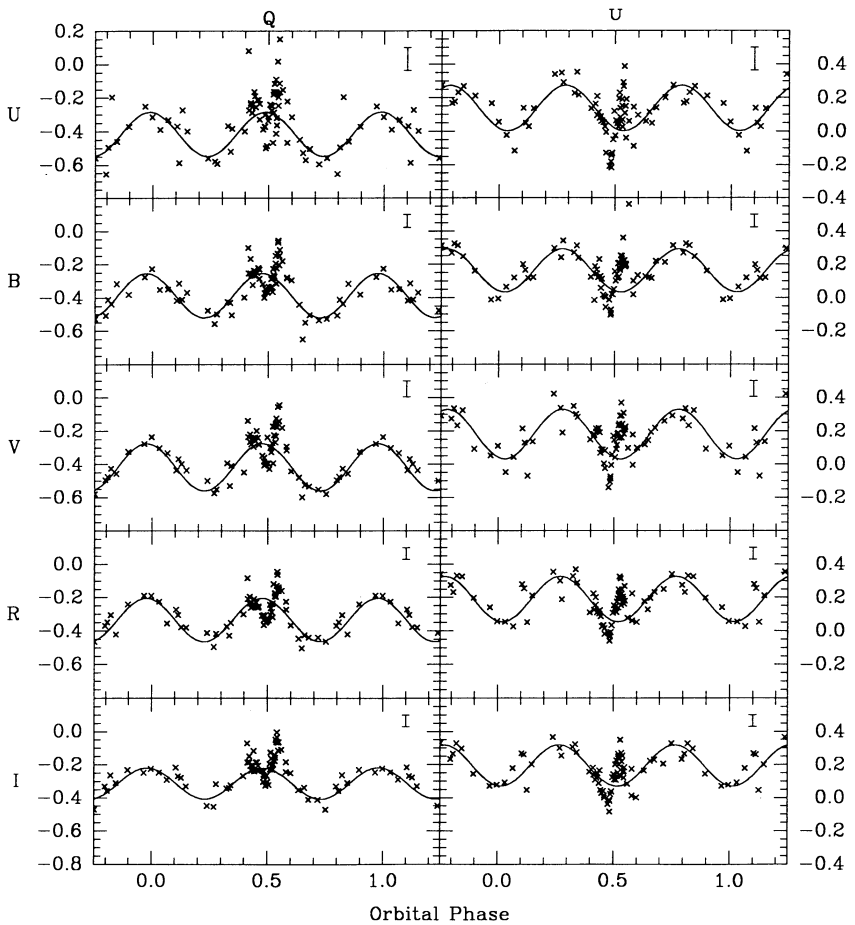

FIG. 2.—*UBVRI* linear polarization observations of V444 Cyg as a function of orbital phase calculated with the ephemeris of Khaliullin (1973). The data have been shifted in abscissa by −0.012 in order to give symmetry and agreement with the polarization model. Typical 2 σ error bars are shown in the top right corner of each plot.

than that found by Robert et al. (1990): 78°.7 ± 0°.5. Its high value is compatible with the deep eclipses. The weighted mean value of the angle of the major axis of the *Q*–*U* locus measured eastwards from the celestial north pole, $\Omega = -41°.8 \pm 3°.8$ or $\Omega = 360° - 41°.8 = 318°.2 \pm 3°.8$, is also compatible with Robert et al.'s (1990) value: 316°.4 ± 0.9.

In Figure 3, we show the deviation of the mean Stokes's parameters from this fitted curve, as a function of orbital phase. The polarization eclipse effect around phase 0.5 is quite clear; it confirms and improves on that found by Robert et al. (1990). Also in Figure 3, we show the light curve of Kron & Gordon (1943), together with ours (with secondary minimum at JD 2,447,767.405). Using the ephemeris of Khaliullin (1973), a shift of −0.017 in light-curve phase is required to make them coincide. Adopting this same ephemeris, Khaliullin et al. (1984) use a set of carefully chosen times of minimum to estimate the change of period of V444 Cyg. In Figure 4*a* we reproduce their Figure 2 illustrating the dependence of the residuals from the linear elements on the Julian Date. The second-order fit yields a rate of period increase of $\dot{P} = 0.202 \pm 0.018$ s yr^{-1}. We have added our new time of minimum to this figure (*filled dot*) and find that it is compatible within the errors with their estimate of the period change. If one uses the ephemeris of Underhill, Grieve, & Louth (1990), a shift of −0.014 is necessary to make

TABLE 2

POLARIMETRIC PARAMETERS OF V444 CYGNI CALCULATED WITH THE POLARIZATION MODEL OF BINARY STARS (EXCLUDING DATA POINTS BETWEEN $\varphi = 0.4$–0.6)

Parameter	*U*	*B*	*V*	*R*	*I*	All Filters
i	80°.2 ± 2°.2	79°.9 ± 1°.7	79°.8 ± 1°.8	81°.6 ± 1°.1	83°.6 ± 1°.7	80°.8 ± 1°.6
Ω	−44°.1 ± 6°.1	−46°.2 ± 4°.0	−43°.4 ± 4°.4	−43°.4 ± 2°.7	−36°.2 ± 3°.4	−41°.8 ± 3°.8
$\tau_0\gamma_3$	(1.72 ± 0.18) × 10^{-3}	(1.71 ± 0.11) × 10^{-3}	(1.89 ± 0.13) × 10^{-3}	(1.78 ± 0.08) × 10^{-3}	(1.51 ± 0.09) × 10^{-3}	(1.68 ± 0.10) × 10^{-3}
$\tau_0\gamma_4$	(−0.29 ± 0.13) × 10^{-3}	(0.02 ± 0.10) × 10^{-3}	(−0.08 ± 0.12) × 10^{-3}	(0.02 ± 0.07) × 10^{-3}	(−0.06 ± 0.09) × 10^{-3}	(−0.05 ± 0.09) × 10^{-3}
λ_2	−4°.7 ± 2°.2	0°.3 ± 1°.7	−1°.3 ± 1°.8	0°.3 ± 1°.1	−1°.2 ± 1°.7	−0°.8 ± 1°.6
A_p	0.18 ± 0.02	0.18 ± 0.01	0.19 ± 0.01	0.18 ± 0.01	0.15 ± 0.02	0.17 ± 0.02

NOTE.—The last column gives the results of a weighted fit to the weighted mean of each of the *UBVRI* data points.

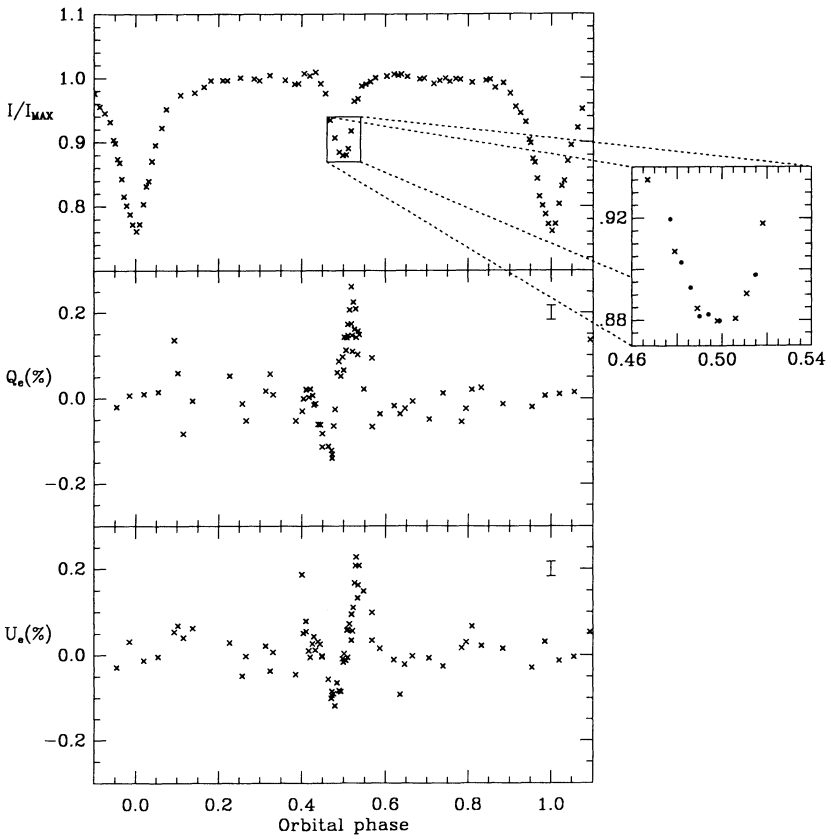

FIG. 3.—(*Bottom two panels*): Deviations of the mean Stokes's parameters from the double-wave BME–type curve (Q_e, U_e) as a function of orbital phase for V444 Cyg. As in Fig. 2, the data are shifted by −0.012 in abscissa. Typical 2 σ error bars are shown in the top right corner of each plot. (*Top panel*): Light curve in the *B* band of Kron & Gordon (1943) (*crosses*) together with our new photometric observations (*filled dots*). A shift of −0.017 in phase is required to make them coincide.

our new photometric light curve coincide with that of Kron & Gordon (1943). Using a different set of times of photometric minimum, Underhill et al. (1990) have also estimated the rate of period change based on their ephemeris. In Figure 4*b*, we have plotted their residuals from the linear elements as a function of Julian Date (their case 2) which yield a much smaller value for the period lengthening, $\dot{P} = 0.088 \pm 0.022$ s yr.[5] Our new time of minimum (*filled dot*) is not incompatible with their period lengthening estimate although their curve is not as well defined and the scatter around the curve is much higher than for that of Khaliullin et al. (1984).

5. MODEL ECLIPSE CALCULATION

In order to model the observed polarization eclipse curves described in the previous section, one must calculate the net degree of polarization produced by scattering of the light from the stars off electrons outside the eclipsed regions described in § 2. As the net polarization should be zero in the absence of eclipses (after subtracting off the double-wave orbital modulation), the degree of polarization produced by the *eclipsed* electrons should have exactly the same value, but with opposite sign. However, the domain of the region containing the noneclipsed electrons is rather complex. Therefore, following Robert et al. (1990), we will calculate instead the net degree of polarization produced by the *eclipsed* electrons as this region is much simpler to describe.

[5] Note that there seems to be a mistake in the error estimates of the period change in Table 4 of Underhill et al. (1990); simple error propagation yields the much higher uncertainty stated here.

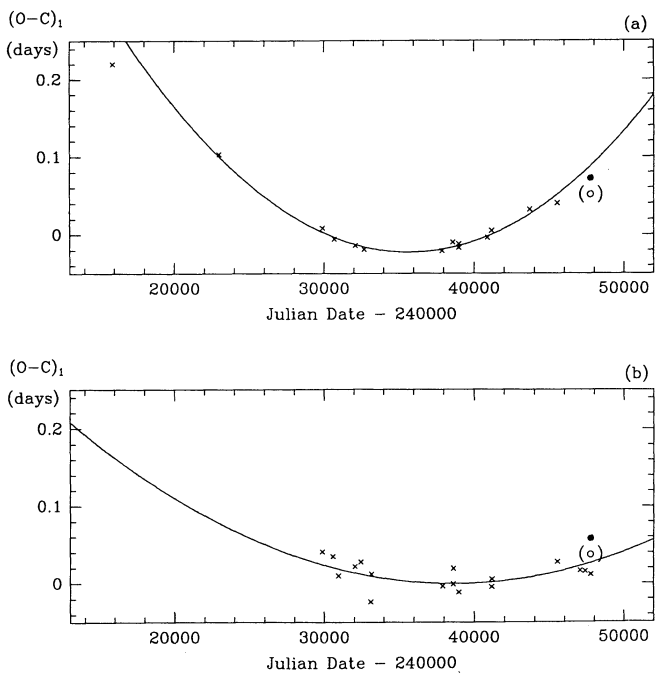

FIG. 4.—Plot of the residuals of the predicted to observed epochs of primary minimum as a function of Julian Date (*crosses*) (*a*) reproduced from Khaliullin et al. (1984) and (*b*) based on data from Underhill et al. (1990). We have added our new estimate for the present data set (*filled dot*) and the value determined from the linear polarization observations (*open circle*) to both graphs.

The calculations presented here are an extension of the model presented by Robert et al. (1990), which is itself based on the general equations developed by BME. In deriving these equations, all of these authors have assumed that the envelope is optically thin and is corotating in the frame of the binary. Therefore our calculations also implicitly include these two assumptions. The present model contains many improvements over the one developed by Robert et al. (1990). In their calculations, these authors have assumed the following:

1. The only important occulted cylinder is that of the O star.
2. The only important light source is the WR star.
3. A spherically symmetric stellar wind is blown from the WR star only.
4. The point source approximation is valid for each star when calculating the polarization.
5. One need only include the region not accessible to the WR-star light due to the disk of the O star (noted A_O above). As mentioned in § 2, this region produces variations which are of the same type as those predicted by the BME model and therefore should not affect the eclipse calculations very much. However, Robert et al. (1990) approximated the cone-shaped occulted region by a cylinder which, in principle, may have introduced a slight error in the calculations.

We have argued in § 2 that assuming only the O-star occulting cylinder to be important is basically a very good approximation. Therefore, we make the same supposition here. For the sake of simplicity, we also assume that only the WR star has a significant wind and that this wind is spherically symmetric. As an improvement to the Robert et al. model, we will allow for the fact that the O star is also an important light contributor for scattered photons. Furthermore, we will avoid making the point light source approximation by including the depolarization factor of Cassinelli et al. (1987) in our model. Finally, as we do not calculate contributions from area A_O (see § 2) we avoid incorrectly approximating the coned-shaped region by a cylinder.

The degree of polarization produced by continuum light scattered off electrons in the cylinder behind the O star is given by

$$Q_e = Q_O + Q_{WR} ,$$
$$U_e = U_O + U_{WR} , \quad (1)$$

where Q_O and U_O are the polarization Stokes's parameters due to the light from the O star, while Q_{WR} and U_{WR} are the contributions from the light of the WR star. In order to facilitate the calculations, we have adopted in our equations a cylindrical coordinate system (x, ρ, ϕ) centered on the O star, which we illustrate in Figure 5. The O star is at the origin of the Cartesian coordinate system xyz and the WR star is at the origin of a second Cartesian coordinate system $x'y'z'$, which is aligned with xyz, but situated at a position $(\Delta x, \Delta y, \Delta z)$ with respect to the position of the O star. The observer is located in direction Ox or Ox'. The distances r_{WR} and r_O between the centers of the WR and O stars, respectively, and a given scattering point P, are shown. Also indicated in this figure are the scattering angles for the O and WR-star light (χ_{WR} and χ_O, respectively) as well as the angles ψ_{WR} between the WR-star light scattering plane and the $x'O'y'$ plane and ψ_O between the O-star light scattering plane and the xOy plane.

According to the theory of BME (supplemented by the depolarization factor of Brown, et al. 1989), the linear polarization

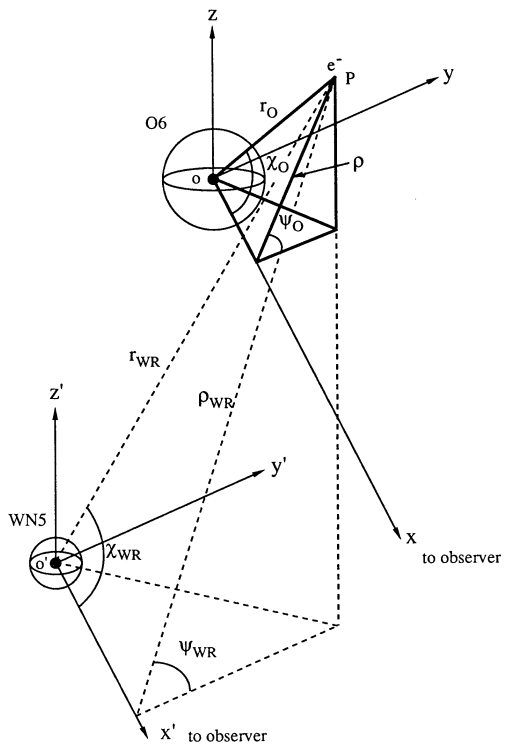

FIG. 5.—Coordinate system adopted in the present calculations (x, ρ, ϕ) centered on the O-star companion. Also shown is another coordinate system (x', ρ', ϕ') centered on the WR star as well as a few useful geometrical relations between the various angles and distances.

Stokes parameters are given by the following expressions:

$$Q_i = -\left(\frac{3\sigma_T}{16\pi}\right) f_i \int_V \frac{n_e(r_{WR})}{r_i^2} D_i \sin^2 \chi_i \cos 2\psi_i \, dV ,$$
$$U_i = -\left(\frac{3\sigma_T}{16\pi}\right) f_i \int_V \frac{n_e(r_{WR})}{r_i^2} D_i \sin^2 \chi_i \sin 2\psi_i \, dV , \quad (2)$$

with i = WR, O.

In this equation, σ_T is the Thomson cross section per electron, f_i is the ratio of the intensity of star i to the total intensity for a given orbital phase, $n_e(r_{WR})$ is the electron number density in the WR wind at a distance r_{WR} from the WR star, D_i is the depolarization factor for star i and $dV = \rho \, d\rho \, dx \, d\phi$ is the element of volume. We express the phase variation of f_i as follows:

$$f_{WR} = \left(\frac{I_{WR}}{I_\phi}\right) = \frac{[1 + 10^{(M_{V*WR} - M_{V*O})/2.5}]^{-1}}{I_\phi / I_m} ,$$
$$f_O = \left(\frac{I_O}{I_\phi}\right) = \frac{[1 + 10^{(M_{V*O} - M_{V*WR})/2.5}]^{-1}}{I_\phi / I_m} . \quad (3)$$

Here I_i is the light intensity and M_{V*i} the absolute magnitude in the V band of star i (i = WR, O), I_ϕ is the total light intensity at phase ϕ, and I_m is the maximum total light intensity between eclipses ($= I_{WR} + I_O$).

For the electron density in the WR wind, we adopt an expression based on mass conservation, $\dot{M} = \text{const} = 4\pi r_{WR}^2 v(r_{WR}) \rho(r_{WR})$, where $v(r_{WR})$ and $\rho(r_{WR})$ refer to the velocity

and density structure of the WR wind:

$$n_e(r_{WR}) = \frac{\alpha\rho(r_{WR})}{m_p} = \frac{\alpha\dot{M}}{4\pi m_p r_{WR}^2 v(r_{WR})} . \quad (4)$$

Here the number of free electrons per nucleon is given by $\alpha = \sum F_i Z_i/N_i$, with, for the ith ion, F_i equal to the number of nucleons in the nucleus, and Z_i equal to the number of free electrons per ion. We will assume that the WR wind mainly consists of He and that He is completely ionized in the region included in these calculations, which implies that $\alpha = \frac{1}{2}$. m_p is the mass of the proton and, as noted above, r_{WR} is the distance from the center of the WR star.

Finally, the depolarization factor for star i is simply given by

$$D_i = \sqrt{1 - R_{i*}^2/r_i^2} , \quad (5)$$

with i = WR, O and where R_{i*} is the radius of star i.

Substituting equations (3) and (5) in equation (2) and using the following geometrical relations:

$$\phi = \frac{\pi}{2} - \psi_O , \quad r_O^2 = \rho^2 + x^2 , \quad \sin\chi_O = \frac{\rho}{(\rho^2 + x^2)^{1/2}}$$

we obtain for the O-star contribution,

$$Q_O = \left(\frac{-3\sigma_T}{16\pi}\right) f_O \int_{-\infty}^{x_s}\int_0^{R_{O*}}\int_0^{2\pi} \frac{n_e(r_{WR})\rho^2}{(\rho^2 + x^2)^2}\sqrt{1 - \frac{R_{O*}^2}{(\rho^2 + x^2)}} \times (-\cos 2\phi)\rho\, dx\, d\rho\, d\phi ,$$

$$U_O = \left(\frac{-3\sigma_T}{16\pi}\right) f_O \int_{-\infty}^{x_s}\int_0^{R_{O*}}\int_0^{2\pi} \frac{n_e(r_{WR})\rho^2}{(\rho^2 + x^2)^2}\sqrt{1 - \frac{R_{O*}^2}{(\rho^2 + x^2)}} \times (+\sin 2\phi)\rho\, dx\, d\rho\, d\phi , \quad (6)$$

where $x_s = (R_{O*}^2 - \rho^2)^{1/2}$.

For the WR star contribution, we again substitute equations (3) and (5) in equation (2) but use the following expression:

$$x' = r_{WR}\cos\chi_{WR} = x + \Delta x ,$$

$$y' = r_{WR}\sin\chi_{WR}\cos\psi_{WR} = \rho\sin\phi + \Delta y ,$$

$$z' = r_{WR}\sin\chi_{WR}\sin\psi_{WR} = \rho\cos\phi + \Delta z ,$$

to finally obtain

$$Q_{WR} = \left(\frac{-3\sigma_T}{16\pi}\right) f_{WR} \int_{-\infty}^{R_{O*}}\int_0^{R_{O*}}\int_0^{2\pi} \frac{n_e(r_{WR})}{r_{WR}^4}\sqrt{1 - \frac{R_{WR*}^2}{r_{WR}^2}} \times [(\rho\sin\phi + \Delta y)^2 - (\rho\cos\phi + \Delta z)^2]\rho\, dx\, d\rho\, d\phi ,$$

$$U_{WR} = \left(\frac{-3\sigma_T}{16\pi}\right) f_{WR} \int_{-\infty}^{R_{O*}}\int_0^{R_{O*}}\int_0^{2\pi} \frac{2n_e(r_{WR})}{r_{WR}^4}\sqrt{1 - \frac{R_{WR*}^2}{r_{WR}^2}} \times [(\rho\sin\phi + \Delta y)(\rho\cos\phi + \Delta z)]\rho\, dx\, d\rho\, d\phi . \quad (7)$$

The position of the O star with respect to the WR star (Δx, Δy, Δz) depends on the orbital separation, a, on the orbital inclination, i, and on the orbital phase, φ, and can be expressed as follows:

$$\Delta x = a\sin i\cos\eta ,$$

$$\Delta y = a\sin\eta ,$$

$$\Delta z = a\cos i\cos\eta ,$$

where $\eta = 2\pi(0.5 - \varphi)$.

Equations (6) and (7) together with equation (4) constitute the base of the present model. Many parameters need to be adopted. We have used a velocity law for the WR-star wind of the type $v(r_{WR}) = v_\infty(1 - R_{WR*}/r_{WR})^\beta$ with $\beta = 0.8$ for O-star winds (Friend & Abbott 1986), although the WN5 component in V444 Cyg also shows a similar value according to the eclipse light curves of Cherepashchuk et al. (1984). For the orbital inclination of the system, we have adopted the value determined by Robert et al. (1990), $i = 78\overset{\circ}{.}7$, which has been derived from the most comprehensive set of linear polarimetric observations outside eclipse obtained to date and is, in any case, compatible with the value in Table 2. This value is in good agreement with the photometric values of Cherepashchuk (1975), $i = 78° \pm 1°$, and Kron & Gordon (1950), $i = 78\overset{\circ}{.}4$. The observed values of Q and U have also been derotated by $-\Omega$ in the Q–U plane, in order to put the new Q axis perpendicular to the projected major axis of the orbital plane. We adopt $\Omega = 316\overset{\circ}{.}4$ from Robert et al. (1990). For the magnitude difference in the V band between the WR and O stars, $\Delta M = M_{V*WR} - M_{V*O}$, we have adopted the same value as Robert et al. (1990), $\Delta M = 1.3$ which is based on magnitude estimates for the O star by Schmidt-Kaler (1982) and for the WR star by Cherepashchuk et al. (1984). The effect of varying this parameter will be discussed in the next section. Finally, the orbital separation of Münch (1950), $a = 40\ R_\odot$, was used and the variation of f_{WR} and f_O as a function of orbital phase was estimated from the light curve of Kron & Gordon (1943).

In the next section, we will describe how we can use the model eclipse calculations presented here to constrain the three main parameters which remain to be determined: the radii of the O (R_{O*}) and WR (R_{WR*}) stars as well as the value of the ratio $\dot{M}/v_\infty$.

6. RESULTS AND DISCUSSION

The contributions of the O and WR stars to the total predicted linear polarization were evaluated separately in order to estimate the relative importance of each. We found that the polarization produced by the scattering of the O-star light off electrons in the WR-star wind which are contained in the O-star shadow is negligible, of the order of 0.5% of the WR-star contribution. This is well below the observational uncertainties and therefore was disregarded in the final models. The low level of the O-star contribution can be understood in terms of the larger distance of the O star to the higher densities of electrons which, according to our assumptions, are found close to the WR-star core. Also, in view of the geometry at eclipse, the photons from the O star are mainly backscattered and the inefficiency of the scattering process at those angles is certainly an important factor toward the low value of the O-star contribution. Therefore, in practice the only significant contribution to the total predicted linear polarization comes from the scattering of the light of the WR star off electrons in the O-star shadow.

The first aspect we have examined is the effect on our calculated models of varying the three parameters R_{WR*}, R_{O*} and $\dot{M}/v_\infty$. As we have assumed that the WR wind is optically thin, we have attempted to exclude from our calculations the region very close to the WR core where the density is sufficiently high to render the envelope optically thick to electron scattering. To do so, we have introduced a cutoff radius, R_c, below which we assume the electron density to be zero. We have considered this cutoff radius as a free parameter and use our calculated

models to constrain it along with the other three parameters listed above. To exclude from our calculations the very high electron density regions near the WR-star surface is not likely to introduce very much error. Indeed in this region, multiple scattering is probably extremely frequent, which has the tendency to eliminate any systematic linear polarization.

Although we have adopted a velocity law with $\beta = 0.8$ (see previous section), we have tested the effect of varying this parameter on the calculated curves. We produced models for values in the interval $\beta = 0.5$–1.0 and found no major differences in the calculated curves. This is most likely explained by the fact that for all these values of β the eclipsed part of the wind has reached a velocity which represents a substantial fraction of the terminal velocity. Therefore the effect of changing the steepness of the velocity law on the density and therefore on our model calculations is minimal.

We have also examined the effect of varying the adopted magnitude difference between the two stars, $\Delta M = M_{V*\mathrm{WR}} - M_{V*\mathrm{O}} = 1.3$. We estimate from equations (3) and (7) that if one adopts a magnitude difference of $\Delta M = -1.1$ as suggested by Hamann & Schwarz (1992) (their best model [B]) our mass-loss rates will have to be decreased by a factor of ~ 3. If however we adopt $\Delta M = 1.5$ (Lundström & Stenholm 1984) our estimated mass-loss rates will have to be increased by a factor of ~ 1.2.

Figure 6 illustrates the effect of varying the radius of the O star on the linear polarimetric Stokes parameters Q_e and U_e. Three different models are presented in which the radius of the WR star and the cutoff radius are kept constant ($R_{\mathrm{WR}*} = 2.9\ R_\odot$, $R_c = 4.8\ R_\odot$) and where $R_{\mathrm{O}*}$ takes the values 8.0, 8.5, and 9.5 $R_\odot$. The value of $K = 100(3\sigma_T/16\pi)(\dot{M}/8\pi m_p v_\infty)$ which controls simultaneously the absolute amplitude of the variations in Q_e and U_e is adjusted accordingly. These three curves are superposed on the observational data points described in § 4. Note that a shift in phase of $\Delta\varphi = -0.012$ compared to the linear ephemeris of Khaliullin (1973) is necessary to optimize the fit. This value is slightly smaller than the value obtained from the light curve ($\Delta\varphi = -0.017$).

It is clear from Figure 6 that the main effect of varying the O-star radius on the Q_e parameter is to change its amplitude and to shift the variations slightly in ordinate. For the U_e parameter, the effect of varying the O-star radius is to change the separation in orbital phase between the minimum and maximum values. This is the only parameter which has an effect on this separation and therefore the O-star radius is relatively well constrained. We adopt a value of $R_{\mathrm{O}*} = 8.5\ R_\odot$ as the best simultaneous fit to both parameters. From Figure 6, we estimate the uncertainty to be $\sim \pm 1\ R_\odot$.

Adopting this value for the O-star radius, we now examine the effect of varying the value of the cutoff radius, R_c. In Figure 7, three model curves calculated with $R_{\mathrm{O}*} = 8.5\ R_\odot$ and $R_{\mathrm{WR}*} = 2.9\ R_\odot$ with $R_c = 4.0$, 4.6, and 5.0 $R_\odot$ are superposed on the observational data points. The consequences of varying the cutoff radius are to change the amplitude of the Q_e parameter as well as the total width in orbital phase of the U_e parameter. From Figure 7, we adopt a value of $R_c = 4.6 \pm 0.5\ R_\odot$. Again, the value of K is modified in consequence. Note that it is difficult to obtain a satisfactory fit to the U_e parameter for phases larger than ~ 0.52. This is caused by the fact that although the models produce curves which are perfectly antisymmetric, the observational polarimetric eclipse in the U parameter is slightly narrower for phases greater than 0.5 than for phases less than 0.5. It is not clear at present what causes this departure from perfect antisymmetry for U in the observa-

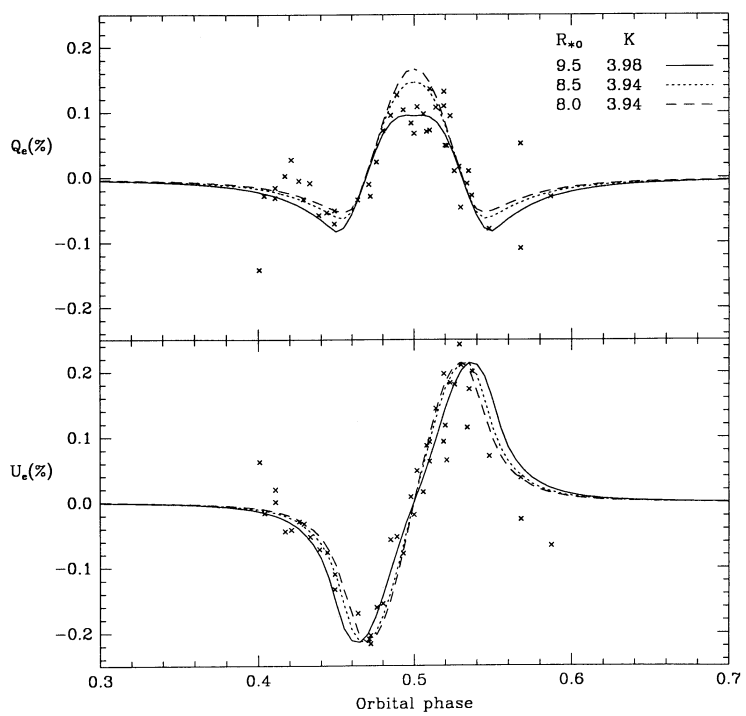

FIG. 6.—Illustration of the effect of varying the radius of the O star, $R_{\mathrm{O}*}$, on the calculated linear polarization curves. All models were calculated using $R_{\mathrm{WR}*} = 2.9\ R_\odot$ and $R_c = 4.8\ R_\odot$. The constant K controls simultaneously the absolute amplitude of variation of Q_e and U_e. The crosses represent the data from Fig. 3 which have been derotated by an angle of 316°.4 and shifted in abscissa by −0.012.

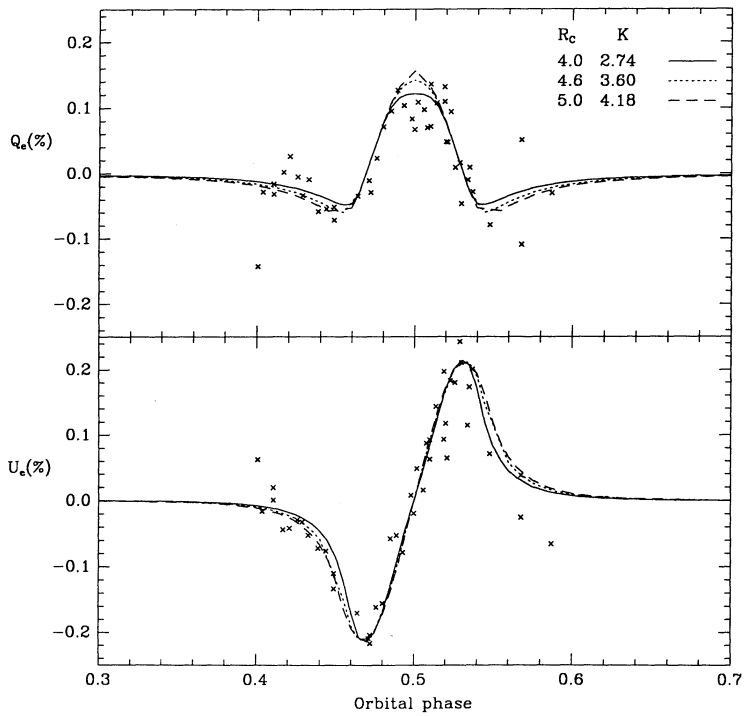

FIG. 7.—Effect of varying the critical radius, R_c, on the predicted polarization curves. All models were calculated using $R_{O*} = 8.5\ R_\odot$ and $R_{WR*} = 2.9\ R_\odot$. Other details as in Fig. 6.

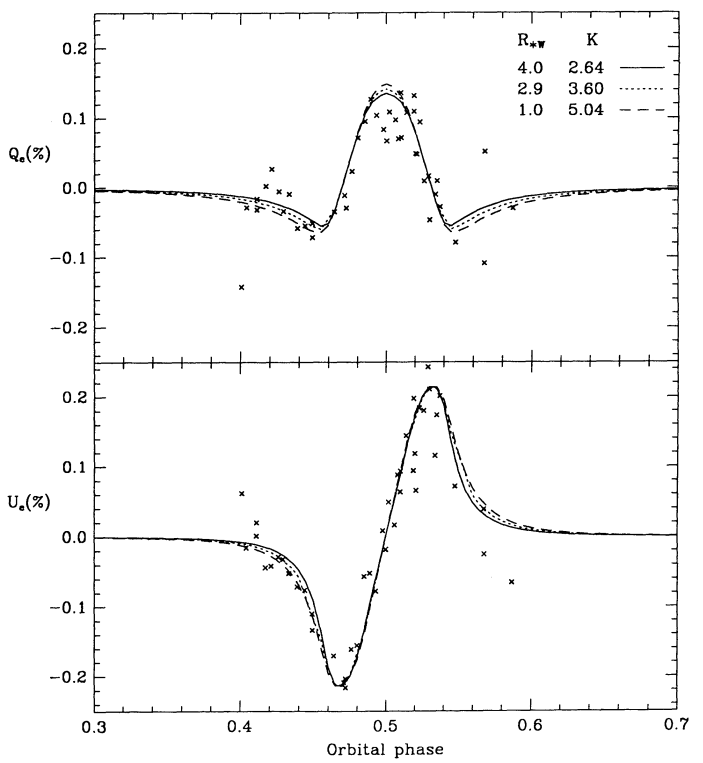

FIG. 8.—Effect of varying the radius of the WR star, R_{WR*}, on the predicted polarization curves. All models were calculated using $R_{O*} = 8.5\ R_\odot$ and $R_c = 4.6\ R_\odot$. Other details as in Fig. 6.

tional data. Perhaps the WR wind is not perfectly spherically symmetric (e.g., due to orbital motion) causing some slight discrepancy.

Finally, the effect of changing the WR star radius, R_{WR*}, is illustrated in Figure 8. The three curves which are shown have been calculated with $R_{O*} = 8.5\ R_\odot$, $R_c = 4.6\ R_\odot$, and $R_{WR*} =$ 1.0, 2.9, and 4.0 $R_\odot$. The effect on the Q_e and U_e parameters of changing the WR-star radius is very similar to that of changing the cutoff radius around the WR star but is much smaller. This is not completely surprising as this parameter intervenes only in the velocity law of the WR wind and therefore in the electron density as a function of distance from the WR star. Changing the WR-star radius only slightly affects the steepness of the velocity law and therefore of the electron density near the WR surface. At the cutoff radius, the resulting change in density for these values of R_{WR*} is apparently very small. Nevertheless, we can conclude from Figure 8 that $R_{WR*} < 4\ R_\odot$. The value determined from the multiwavelength photometric eclipse by Cherepashchuk et al. (1984), 2.9 $R_\odot$, is perfectly consistent with our results and therefore we adopt this much better constrained value in our final model.

Figure 9 shows the final model fit to the observations using the parameters discussed above ($R_{O*} = 8.5\ R_\odot$, $R_c = 4.6\ R_\odot$, and $R_{WR*} = 2.9\ R_\odot$). The resulting value of K is 3.60. In Figure 10 we have superposed this model curve to the observations for each individual waveband observed (U, B, V, R, I) for the two Stokes parameters Q and U as a function of orbital phase. Within the errors, no significant wavelength dependence can be observed, confirming electron scattering as the dominant process producing the linear polarization variations.

The value of the scaling constant in the adopted model, $K = 3.60$, corresponds to $\dot{M}/v_\infty = 1.33 \times 10^{-16}\ M_\odot\ \mathrm{km}^{-1}$. Adopting a wind terminal velocity of 1785 km s^{-1}, determined from the violet limit of the saturated absorption trough of the C IV λ1550 UV resonance doublet (Prinja, Barlow, & Howarth 1990), one finds a mass-loss rate of $\dot{M} = 0.75 \times 10^{-5}\ M_\odot\ \mathrm{yr}^{-1}$. Mass-loss rates can also be estimated from the double-wave binary-induced polarization curves; using this technique, St-Louis et al. (1988) found for V444 Cyg, $\dot{M} = 0.9 \times 10^{-5}\ M_\odot\ \mathrm{yr}^{-1}$. However, they had adopted a terminal velocity of 2500 km s^{-1}. Using the terminal velocity of Prinja et al. (1990), as we have done in the present model, one obtains instead $\dot{M} = 0.6 \times 10^{-5}\ M_\odot\ \mathrm{yr}^{-1}$, which is very similar to our value determined from the polarization eclipse. This gives us some confidence in our result because although both methods rely on the same basic hypotheses, they do not sample identical parts of the wind and are thus fairly independent. These estimates of the mass-loss rate are, however, based on model assumptions and are likely to be affected if these were to change.

These estimates of the mass-loss rate of V444 Cyg can be compared with that obtained from the free-free radio flux of Bieging, Abbott, & Churchwell (1982) and the formula of Wright and Barlow (1975). Prinja et al. (1990) (using their newly estimated terminal velocity of 1785 km s^{-1}) find for V444 Cyg, $\dot{M} = 2.4 \times 10^{-5}\ M_\odot\ \mathrm{yr}^{-1}$, almost 3 times higher than our polarization estimates. Howarth & Schmutz (1992) provide another independent estimate of the mass-loss rate of V444 Cyg from a high-quality near-IR spectrum; modeling of the He I λ10830 Å line yields a rate in the range $\dot{M} = 2.0$–$5.0 \times 10^{-5}\ M_\odot\ \mathrm{yr}^{-1}$, depending on what magnitude difference between the O and WR stars they adopt. This is consistent with the value obtained from the radio flux and significantly higher than our polarization estimates.

From a consistent model of the light curve and the helium spectrum, Hamann & Schwarz (1992) find a mass-loss rate for

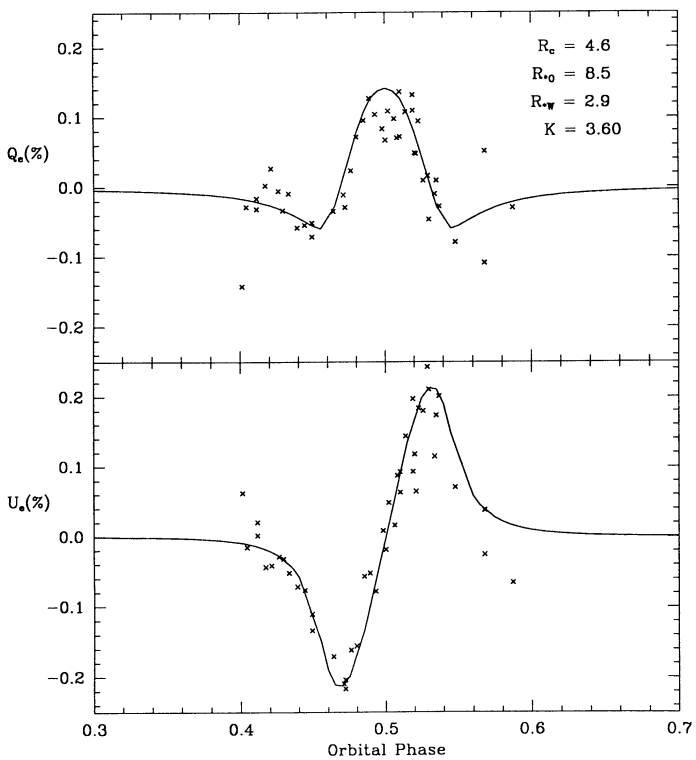

FIG. 9.—Final model fit to the observations using $R_{O*} = 8.5\ R_\odot$, $R_c = 4.6\ R_\odot$, and $R_{WR*} = 2.9\ R_\odot$. Details as in Fig. 6.

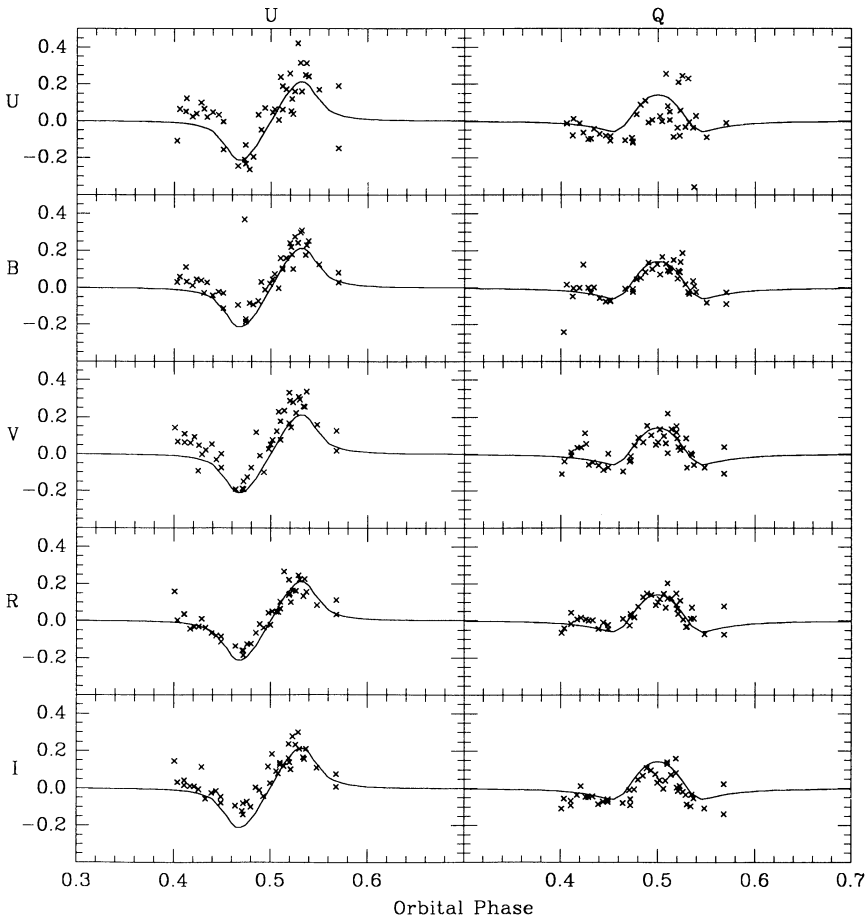

FIG. 10.—Adopted model fit superposed on the polarimetric observations of the two Stokes parameters Q_e and U_e for each individual waveband (*UBVRI*)

the WR component in V444 Cyg of $\dot{M} = 1.26 \times 10^{-5}\ M_\odot\ \mathrm{yr}^{-1}$ which is intermediate between the radio/infrared and our polarization estimates. However, this value cannot be directly compared to ours as we have not adopted the same magnitude difference between the O and WR stars as they have deduced from their analysis ($\Delta M = -1.1$ mag). In fact, as mentioned above, if we adopt their magnitude difference, our mass-loss rates will be reduced by a factor of ~ 3 and the two estimates would become very different. Furthermore, this would also widen even more the disparity between our polarization mass-loss rates and the free-free radio and infrared spectroscopic estimates.

The magnitude difference between the two stars estimated by Hamann & Schwarz (1992) is in fact contrary to all previous determinations, as it identifies the WR star as the brightest component. There are many reasons why we have not adopted Hamann & Schwarz's (1992) estimate for the magnitude difference. First, their result is not in agreement with mean absolute magnitudes for single WN5 and O6 stars found in the literature. For WN5 stars, van der Hucht et al. (1988) find an average absolute magnitude of $M_V = -4.8$ while for O6 stars Howarth & Prinja (1989) find a mean value of $M_V = -5.2$ for a main-sequence star and -6.6 for a supergiant. This gives $\Delta M_V = +0.4$ to $+1.8$ between the two stars, far from Hamann & Schwarz's (1992) value of -1.1. Furthermore, in their best model solution (B), Hamann & Schwarz (1992) obtain a value for the O-star radius which is surprisingly low ($R_{O*} = 3.76\ R_\odot$). Mean values from the literature for O6 stars are at least a factor of 3 higher than this (e.g., Howarth & Prinja 1989). Hamann & Schwarz (1992) argue from an H-R diagram analysis that their model might have underestimated the luminosities of both stars by a factor of 3. Assuming this error is unlikely to be due to incorrect temperatures, they suggest that the stellar radii should perhaps be arbitrarily doubled. This should bring their O-star radius estimates much closer to mean observed values but would result in a WR-star radius estimate of $R = 12\ R_\odot$, which is extremely high and in clear disagreement with our estimated value (upper limit) and other values determined by previous authors (e.g., Cherepashchuk et al. 1984; De Greve & Doom 1988).

Naturally the determination of the stellar radii and of the magnitudes of the stars are intimately linked, and therefore we have preferred to adopt a more standard value for the magnitude difference. Note however that this choice solely affects the absolute value of our mass-loss rate estimate and has no influence on the basic results of this paper. In particular, whatever ΔM_V we adopt still results in a large difference between our mass-loss rate estimates and those determined from the free-free radio fluxes or the infrared spectroscopic observations. The methods could perhaps be reconciled if the distance to V444 Cyg was significantly smaller than previously thought, as this would lower the values determined by the two latter methods. Such a small distance is indeed suggested by the model of Hamann & Schwarz (1992), $d = 720$ pc (instead of

$d = 1720$ pc from cluster membership in Be 86 by Lundström & Stenholm 1984), but the authors themselves stress the fact that their magnitude estimates are most likely too faint and therefore that the distance to the system they obtain is too small.

One can also deduce a dynamical mass-loss rate for V444 Cyg from the orbital period change. The shift of -0.017 in phase that we have found between our new light curve and that of Kron & Gordon (1943) (see § 4) is compatible with the period change of $\dot{P} = 0.202 \pm 0.018$ s yr^{-1} determined by Khaliullin et al. (1984). Assuming a spherically symmetric outflow of matter from the WR star with no mass transfer to the O-type companion, we can convert this period lengthening to a mass-loss rate. Adopting $M_O = 25\ M_\odot$ and $M_{WR} = 10\ M_\odot$ from Münch (1950), we obtain $\dot{M}_{WR} = 1.0 \times 10^{-5}\ M_\odot$ yr^{-1}. This value is similar to those determined from the polarization but at least 2 times smaller than the radio and infrared estimates. From a different set of photometric minima, Underhill et al. (1990) find a much smaller period change ($\dot{P} = 0.088 \pm 0.022$ s yr^{-1}; see § 4) which converts, when using the above masses, into a mass-loss rate for the WR component of $\dot{M}_{WR} = 0.4 \times 10^{-5}\ M_\odot$ yr^{-1}. A mean dynamical value, $\dot{M}_{WR} = 0.7 \times 10^{-5}\ M_\odot$ yr^{-1}, agrees remarkably well with the polarization values ($0.6 \times 10^{-5}\ M_\odot$ yr^{-1} from the double-wave analysis and $0.75 \times 10^{-5}\ M_\odot$ yr^{-1} from the polarization eclipse).

7. CONCLUSIONS

In this paper, we have presented an improved theoretical model to describe the polarization eclipse of the well-known WR binary V444 Cyg. The polarimetric variations in this case are caused by the occultation of varying amounts of scatterers (free electrons) by the core of the O-star companion as a function of orbital phase. We have considered both stars as important light sources.

The linear polarization variations produced by the scattering of the WR-star light were found to dominate compared to those due to the scattering of the O-star radiation. The latter was found to contribute less than half a percent to the total theoretical polarimetric eclipse curve. This can easily be explained by the larger distances of the high densities of electrons in the WR wind to the O-star core and by the fact that the photons from the O star suffer mainly backscattering, which is basically a very inefficient process.

The calculated curves were then compared to an extensive set of linear polarization observations obtained in the *UBVRI* wavebands. No dependence was found on wavelength in agreement with our basic assumption that electron scattering is the main process responsible for the polarization. The comparison between the observed and calculated polarization eclipse curves yielded estimates of the stellar radii (R_{O*}, R_{WR*}) as well as the WR mass-loss rate to terminal velocity ratio ($\dot{M}/v_\infty$). For the O star, we find a radius of $R_{O*} = 8.5 \pm 1\ R_\odot$. This is in agreement with the value obtained by Cherepashchuk et al. (1984), $R_{O*} = 10\ R_\odot$, from an analysis of a set of light curves of V444 Cyg between 2460 Å and 3.5 μm. Howarth & Prinja (1989) have published a list of typical radii for O stars based on a temperature scale obtained from a limited amount of theoretical modeling of high signal-to-noise ratio spectral observations. Based on their values, we conclude that it is most likely that the O-type companion in V444 Cyg is a main-sequence star. A giant star should have a slightly larger radius ($\sim 14\ R_\odot$) whereas a supergiant is completely excluded ($\sim 23\ R_\odot$).

For the WR star we were not able to obtain a very accurate estimate of the core radius as the calculated models are not very sensitive to this parameter. However, we find $R_{WR*} < 4\ R_\odot$ which is compatible with the small value obtained by Cherepashchuk et al. (1984), $R_{WR*} = 2.9\ R_\odot$, from their analysis of the multiwavelength light curve of V444 Cyg. Modeling of high-quality infrared spectra of V444 Cyg by Howarth & Schmutz (1992) yields a radius between 2.5 and 17 $R_\odot$ depending on the brightness ratio adopted.

Finally the comparison between our calculated and observed polarization curves provided us with an estimate of the mass-loss rate to terminal velocity ratio in the WR wind. The best fit yielded a value of $\dot{M}/v_\infty = 1.33 \times 10^{-16}\ M_\odot$ km^{-1} which translates into a mass-loss rate of $\dot{M} = 0.75 \times 10^{-5}\ M_\odot$ yr^{-1} if one adopts a terminal velocity of 1785 km s^{-1}. This agrees well with the value determined from the double-wave BME–type polarization curves by St-Louis et al. (1988), corrected for a new lower v_∞, $\dot{M} = 0.6 \times 10^{-5}\ M_\odot$ yr^{-1}. It is also compatible with the dynamical estimate based on the period change by Khaliullin et al. (1984), and Underhill et al. (1990): $\dot{M} = (1.0 \text{ and } 0.4) \times 10^{-5}\ M_\odot$ yr^{-1}, respectively.

Mass-loss rates for V444 Cyg obtained from free-free radio observations, $\dot{M} = 2.4 \times 10^{-5}\ M_\odot$ yr^{-1} (Prinja et al. 1990), and from modeling of infrared spectral lines, $\dot{M} = 2.0$–$5.0 \times 10^{-5}\ M_\odot$ yr^{-1} (Howarth & Schmutz 1992), are at least 3 times as large as our new estimate. However, these values are based on the hypothesis that the winds of WR stars are homogeneous. Now there is growing evidence that this assumption is incorrect and that the winds of WR stars are highly structured and variable. Observations reveal intrinsic variability in optical photometry, polarimetry, and spectroscopy (e.g., Moffat & Robert 1991, 1992) as well as in ultraviolet spectroscopy (e.g., St-Louis 1992). Theoretical models describing the development of shocks and instabilities in stellar winds have been described by Owocki, Castor, & Rybicki (1988). Hillier (1991b) has investigated the influence of density inhomogeneities in the winds of hot stars on predicted line profiles and found that line strengths in agreement with observations can be produced but for lower mass-loss rates than for homogeneous winds. This is mainly because nonresonance emission line strengths depend on the *square* of the density and therefore *if the wind is more concentrated in clumps the mass-loss rates must be decreased in order to maintain the same line flux.* Free-free radio emission also depends on the square of the density, and therefore it is not totally unexpected that the mass-loss rates for V444 Cyg determined from the radio fluxes and on modeling of infrared spectral lines agree. Both techniques to determine mass-loss rates based on the modeling of polarimetric variations also assume a homogeneous wind but in these cases the mass-loss rates depend linearly on the density. The effect of an inhomogeneous wind is therefore irrelevant providing the observed electron scattering is optically thin. The mass-loss rates based on the polarization should therefore be more reliable in that respect.

If all hot stars have clumpy winds and V444 Cyg is not untypical, the above results imply that all mass-loss rates based on free-free or nonresonance line emission will have to be significantly reduced. Clearly, more reliable dynamical estimates of mass-loss rates in other binaries would be highly desirable. Obtaining accurate mass-loss rates is extremely important in, for example, stellar wind model calculations and estimates of the enrichment of the interstellar medium.

The polarization techniques to determine mass-loss rates are

admittedly based on several assumptions. One of these is to consider that a spherically symmetric wind is blown from the WR star only. For V444 Cyg there is evidence that the O star also has a significant wind (although it is still 10 times weaker in mass-loss rate than that of the WR star) and that in fact both outflows are colliding forming a coned-shaped interaction region (Shore & Brown 1988; Luo, McCray, & MacLow 1990; Stevens, Blondin, & Pollock 1992). There is also evidence for colliding winds in the WR binary γ Vel from a study of ultraviolet line-profile variability as a function of orbital phase (St-Louis, Willis, & Stevens 1993). It is not clear what the effect of considering a nonspherically symmetric wind for the WR star would be on the theoretical polarization variation curves. We plan to investigate this issue in a future publication.

We would like to thank K. A. van der Hucht for useful comments. N. St-Louis and A. F. J. Moffat wish to thank the Natural Sciences and Engineering Research Council (NSERC) of Canada and the Fonds pour la Formation de Chercheurs et l'Aide à la Recherche (FCAR) of Québec for financial support.

REFERENCES

Bieging, J. H., Abbott, D. C., & Churchwell, E. B. 1982, ApJ, 263, 207
Brown, J. C., Aspin, C., Simmons, J. F. L., & McLean, I. S. 1982, MNRAS, 198, 787.
Brown, J. C., Carlaw, V. A., & Cassinelli, J. P. 1989, ApJ, 344, 341
Brown, J. C., & Fox, G. K. 1989, ApJ, 347, 468
Brown, J. C., McLean, I. S., & Emslie, A. G. 1978, A&A, 68, 415 (BME)
Cassinelli, J. P., Nordsieck, K. H., & Murison, M. A. 1987, ApJ, 317, 290
Chandrasekhar, S. 1946, ApJ, 103, 365
Cherepashchuk, A. M. 1975, Soviet Astron., 19, 47
Cherepashchuk, A. M., Eaton, J. A., & Khaliullin, Kh. F. 1984, ApJ, 281, 774
De Greve, I. P., & Doom, C. 1988, A&A, 200, 79
Drissen, L., Lamontagne, R., Moffat, A. F. J., Bastien, P., & Séguin, M. 1986a, ApJ, 304, 188
Drissen, L., Moffat, A. F. J., Bastien, P., Lamontagne, R., & Tapia, S. 1986b, ApJ, 306, 215
Drissen, L., St-Louis, N., Moffat, A. F. J., & Bastien, P. 1987, ApJ, 322, 888
Fox, G. K. 1992, MNRAS, in press
Fox, G. K., & Brown, J. C. 1991, ApJ, 375, 300
Friend, D. B., & Abbott, D. C. 1986, ApJ, 311, 701
Hamann, W.-R., Leuenhagen, U., Koesterke, L., & Wessolowski, U. 1992, ApJ, 255, 200
Hamann, W.-R., & Schwarz, E. 1992, A&A, 261, 523
Hillier, D. J. 1989, ApJ, 347, 392
———. 1991a, in IAU Symp. 143, Wolf-Rayet Stars and Interrelations with Other Massive Stars in Galaxies, ed. K. A. van der Hucht & B. Hidayat (Dordrecht: Kluwer), 59
———. 1991b, A&A, 247, 455
Howarth, I. D., & Prinja, R. K. 1989, ApJS, 69, 527
Howarth, I. D., & Schmutz, W. 1992, A&A, 261, 503
Khaliullin, Kh. F. 1973, Perem. Zvezdy, 19, 73
Khaliullin, Kh. F., Khaliullina, A. I., & Cherepashchuk, A. M. 1984, Soviet Astron. Lett., 10, 250
Korhonen, T., Piirola, V., & Reiz, A. 1984, ESO Messenger, No. 38
Kron, G. E., & Gordon, K. C. 1943, ApJ, 97, 311
———. 1950, ApJ, 111, 454
Luna, H. C. 1982, PASP, 94, 695
———. 1985, Rev. Mexicana Astron. Af., 10, 267
Lundström, I., & Stenholm, B. 1984, A&A, 58, 163
Luo, D., McCray, R., & MacLow, M.-M. 1990, ApJ, 362, 267
Moffat, A. F. J., & Piirola, V. 1993, ApJ, in press
Moffat, A. F. J., & Robert, C. 1991, in IAU Symp. 143, Wolf-Rayet Stars and Interrelations with Other Massive Stars in Galaxies, ed. K. A. van der Hucht & B. Hidayat (Dordrecht: Kluwer), 109
———. 1992, in Nonisotropic and Variable Outflows from Stars, ed. L. Drissen, C. Leitherer, & A. Nota (ASP Conf. Ser. 22), 203
Moffat, A. F. J., & Shara, M. 1986, AJ, 92, 952
Münch, G. 1950, ApJ, 112, 266
Owocki, S. P., Castor, J. I., & Rybicki, G. B. 1988, ApJ, 335, 914
Piirola, V. 1980, A&A, 90, 48
———. 1988, in Polarized Radiation of Circumstellar Origin, ed. G. V. Coyne et al. (Vatican City State: Vatican Observatory), 735
Piirola, V., & Linnaluoto, S. 1988, in Polarized Radiation of Circumstellar Origin, ed. G. V. Coyne et al. (Vatican City State: Vatican Observatory), 655
Prinja, R. K., Barlow, M. J., & Howarth, I. D. 1990, ApJ, 361, 607
Robert, C., Moffat, A. F. J., Bastien., P., Drissen, L., & St-Louis, N. 1989, ApJ, 347, 1034
Robert, C., Moffat, A. F. J., Bastien., P., St-Louis, N., & Drissen, L. 1990, ApJ, 359, 211
Rudy, R. J., & Kemp, J. C. 1978, ApJ, 221, 200
Schmidt-Kaler, Th. 1982, in Numerical Data and Functional Relationships in Science and Technology, ed. K. Scaiffers & H. H. Voigt (Berlin: Springer), 1
Schmutz, W. 1991, in IAU Symp. 143, Wolf-Rayet Stars and Interrelations with Other Massive Stars in Galaxies, ed. K. A. van der Hucht & B. Hidayat (Dordrecht: Kluwer), 39
Schulte-Ladbeck, R. E., & van der Hucht, K. A. 1989, ApJ, 337, 872
Shore, S., & Brown, D. N. 1988, ApJ, 334, 1021
Shulov, O. S. 1967, Astrofizika 3, 233
Stevens, I. R., Blondin, J. M., & Pollock, A. M. T. 1992, ApJ, 386, 265
St-Louis, N. 1992, in Nonisotropic and Variable Outflows from Stars, ed. L. Drissen, C. Leitherer, & A. Nota (ASP Conf. Ser. 22), 229
St-Louis, N., Drissen, L., Moffat, A. F. J., Bastien, P., & Tapia, S. 1987, ApJ, 322, 870
St-Louis, N., Moffat, A. F. J., Drissen, L., Bastien, P., & Robert, C. 1988, ApJ, 330, 286
St-Louis, N., Willis, A. J. W., & Stevens, I. R. 1993, ApJ, submitted
Underhill, A. B., Grieve, G. R., & Louth, H. 1990, PASP, 102, 749
van der Hucht, K. A., Hidayat, B., Admiranto, A. G., Supelli, K. R., & Doom, C. 1988, A&A, 199, 217
Wright, A. E., & Barlow, M. J. 1975, MNRAS, 170, 41